Journal of Solid State Chemistry 269 (2019) 553–557

Contents lists available at ScienceDirect

Journal of Solid State Chemistry

journal homepage: www.elsevier.com/locate/jssc

One-dimensional tellurium chains: Crystal structure and thermodynamic properties of $PrCu_xTe_2$ (x ~ 0.45)

Ryan Baumbach[a], Luis Balicas[a], Gregory T. McCandless[b], Paola Sotelo[d], Qiu R. Zhang[a], Jess Evans[c], Dino Camdzic[d], Thomas J. Martin[b], Julia Y. Chan[b], Robin T. Macaluso[c,d,*]

[a] National High Magnetic Field Laboratory, Florida State University, Tallahassee, FL 32306, United States
[b] Department of Chemistry and Biochemistry, University of Texas at Dallas, Richardson, TX 75080, United States
[c] Department of Chemistry and Biochemistry, University of Northern Colorado, Greeley, CO 80639, United States
[d] Department of Chemistry and Biochemistry, The University of Texas at Arlington, TX 76019, United States

ARTICLE INFO

Keywords:
$PrCu_xTe_2$
Semiconductor
Crystal growth
Disorder

ABSTRACT

X-ray diffraction, crystal structure, magnetization, and heat capacity results are presented for the rare earth – chalcogenide ternary system $PrCu_{0.45}Te_2$ and its non-4*f* analogue $LaCu_{0.40}Te_2$. The crystal structure of $PrCu_{0.45}Te_2$ is characterized by chains of edge and corner-sharing $CuTe_4$ tetrahedra and Pr centered in polyhedra comprised of Cu and Te. The Cu site is partially occupied and exhibits signatures of local disorder. Magnetic susceptibility measurements show a Curie-Weiss temperature dependence consistent with a Pr^{3+} state. No magnetic ordering is observed down to 1.8 K, but the negative Curie-Weiss temperature suggests an antiferromagnetic exchange interaction. Importantly, the low temperature heat capacity of $PrCu_{0.45}Te_2$ is strongly enhanced by comparison to $LaCu_{0.40}Te_2$, suggesting that there is a build-up of entropy that is associated with the 4f-electrons from the Pr^{3+} ions. These features reveal possible spin frustration behavior and introduce this family of materials as a template for studying new phenomenon.

1. Introduction

The study of low-dimensional solids is of recent interest due to their fascinating electrical, magnetic, optical and thermal properties. The vast bonding motifs of chalcogenides offer a platform to investigate the relationships between dimensionality and physical properties [1–5]. Tellurium-containing intermetallic compounds are known for their charge density waves [6,7] [8] and are strong candidates for mixed conductor, phase switching materials [2,9] and thermoelectrics [10–12]. Recently, WTe_2 has been shown to exhibit extremely large magnetoresistance (452,000%) [13] and superconductivity upon application of pressure [14], and more recently, dichalcogenides such as WTe_2, γ-$MoTe_2$, and $PdTe_2$, to correspond to realizations of Weyl and Dirac semiconductors [15–19].

The covalent nature of one-dimensional telluride chains can lead to low-dimensional, anisotropic behavior [4], and reversible redox switching by electrochemical routes [20]. Quasi one-dimensional structural $PdTe_4$ units in $Ta_4Pd_3Te_{16}$ leads to superconductivity [21]. Other examples of one-dimensional Te chains include $Ba_2Cu_{4-x}Te_5$ [22], $CsTiUTe_5$ [23], $CsTh_2Te_6$ [24] and $Gd_3Cu_2Te_7$ [25]. One-dimensional Te chains are expected to result in metallic behavior; however, many compounds such as $LnCu_xTe_2$ (Ln = La, Nd, Sm, Gd, Dy; $x < 0.4$) [26], exhibit semiconducting behavior. Many such materials are also rich environments to study the influence of the f-electron state on electrical transport and thermodynamic properties. For instance, both CeSb [27] and CeSbSe [28], which crystallize in distinct structures, exhibit devil's staircase magnetic behavior that results from a complex interplay between the f-states and the low charge carrier densities of these systems. In addition, the recent work on CeSbTe has been shown to be a first nonsymmorphic magnetic topological semimetal [29].

In this work, we present the synthesis, crystal structure, magnetic properties, and heat capacity of $PrCu_{0.45}Te_2$. The crystal structure is characterized by $CuTe_4$ tetrahedral units that are connected along the *c*-axis through a quasi-one dimensional network of Te atoms. The lanthanide atoms are arranged in bicapped trigonal prisms that are composed of Te atoms, where the nearest neighbor lanthanide distance is ~ 4.5 Å, i.e., larger than the Hill limit. There is strong disorder on the Cu site that is associated with partial filling. A Curie-Weiss temperature dependence is observed in magnetic susceptibility measurements, revealing that the Pr ions are in the magnetic trivalent state. No magnetic ordering is observed down to 1.8 K, but the negative Curie-Weiss temperature suggests an antiferromagnetic exchange interac-

* Corresponding author at: Department of Chemistry and Biochemistry, The University of Texas at Arlington, TX 76019, United States.
E-mail address: robin.macaluso@uta.edu (R.T. Macaluso).

https://doi.org/10.1016/j.jssc.2018.10.008
Received 27 August 2018; Received in revised form 2 October 2018; Accepted 7 October 2018
Available online 21 October 2018
0022-4596/

tion. The low temperature heat capacity of $PrCu_{0.45}Te_2$ is strongly enhanced in comparison to $LaCu_{0.40}Te_2$, suggesting that there is a build-up of entropy that is associated with the free spins of the 4f-electrons from the Pr^{3+} ions. This reveals possible spin frustration behavior and brings new interest to this family of materials.

2. Experimental

2.1. Synthetic procedures

Single crystals of $PrCu_{0.45}Te_2$ and $LaCu_{0.40}Te_2$ were grown from their constituent elements. Pr/La (rod, 99.9%) were filed inside of a N_2-filled glove box while Cu (shot, 99.999%), and Te (shot, 99.5%) were used as received. The crystal growth was accomplished in two steps. In the first step, a mixture of 1 mol Pr: 2 mol Cu: 3 mol Te were placed in an alumina crucible. The crucible and its contents were subsequently placed in an amorphous silica tube, evacuated and backfilled with of Ar three times before a final evacuation and sealing using a hydrogen torch. The sealed vessel was then heated to 950 °C at a rate of 0.4 °C/min and dwelled there for 1 h before being cooled to room temperature at a rate of 0.1 °C/min. The resulting powder was then ground with excess KI in an agate mortar and pestle for the second step. The mixture was placed in an amorphous silica tube, evacuated and backfilled with of Ar three times before a final evacuation and sealing using a hydrogen torch. The sealed vessel was then heated to 950 °C at a rate of 0.4 °C/min and dwelled there for 72 h before being cooled to 300 °C at a rate of 0.1 °C/min. The sample was removed from the furnace after dwelling at 300 °C for at least 24 h. The synthesis produced black single crystals of $PrCu_{0.45}Te_2$ with lengths ranging from ~ 0.75 to ~ 2.0 mm and a yield of approximately 60% and black single crystals of $LaCu_{0.40}Te_2$ single crystals with dimensions < 1 mm. Crystals were soaked in distilled water to remove excess KI.

Alternatively, powders of $LaCu_{0.40}Te_2$ were produced by placing a mixture of 1 mol La: 2 mol Cu: 2 mol Te in an alumina crucible and subsequently into an amorphous silica tube. The tube was then evacuated and backfilled with of Ar three times before a final evacuation and sealing using a hydrogen torch. The sealed vessel was then heated to 1050 °C at a rate of 0.8 °C/min and dwelled there for 24 h before being cooled to 600 °C at a rate of 0.1 °C/min.

2.2. Elemental analysis

Single crystals of $PrCu_{0.45}Te_2$ were characterized by electron dispersive spectroscopy (EDS) using a JEOL JSM-6610LV microscope with JEOL GUI Software package and an Oxford Instruments INCA Energy 250 spectrometer with an X-Max 20 detector operated with Inca Micro Analysis Suite. Selected crystals were arranged on double-sided carbon tape adhered to an aluminum sample puck. Each crystal was cleaved to expose inner portions to acquire more accurate elemental analysis of the bulk sample and to avoid erroneous readings due to any surface impurities. Several spots on each crystal were analyzed for 45 s, the results from five measurements were averaged, and atomic ratios were normalized to praseodymium. The resulting elemental composition of the sample is $Pr_{1.00(1)}Cu_{0.47(8)}Te_{2.06(4)}$, similar to the composition obtained from single-crystal X-ray diffraction.

2.3. Powder and single crystal X-ray diffraction

Powder X-ray diffraction data was collected on ground single crystals of $LaCu_{0.40}Te_2$ using a Bruker D8 Advance powder X-ray diffractometer equipped with a LYNXEYE XE detector using a Cu Kα radiation source (λ = 1.54184 Å). The powder pattern is included in Supplementary information.

A single-crystal fragment of $PrCu_{0.45}Te_2$ was cut into a suitable size ($0.02 \times 0.08 \times 0.12\ mm^3$) and mounted on a glass fiber with epoxy.

Table 1
Crystallographic data and structure refinement for $PrCu_{0.45}Te_2$.

Space group	*Pbcm*
a (Å)	7.652(2)
b (Å)	8.451(4)
c (Å)	6.234(1)
V (Å^3)	403.2(2)
Z	4
Crystal size (mm^3)	0.02 × 0.08 × 0.12
Temperature (K)	299
θ Range (°)	2.7–30.5
μ (mm^{-1})	28.30
Collected reflections	5471
Unique reflections	642
R_{int}	0.039
h	$-10 \le h \le 10$
k	$-10 \le k \le 11$
l	$-7 \le l \le 8$
$\Delta\rho_{max}$ (e Å^{-3})	2.05
$\Delta\rho_{min}$ (e Å^{-3})	−1.19
GoF	1.21
Extinction coefficient	0.0082(4)
[a]R_1 for $F^2 > 2\sigma(F^2)$	0.0195
[b]w$R_2(F^2)$	0.0476

[a] $R_1 = \sum ||F_0|-|F_c|| / \sum |F_0|$.

[b] $wR_2 = \{\sum [w(F_0^2 - F_c^2)^2] / \sum [w(F_0^2)^2]\}^{1/2}$.

Data sets were collected on a Bruker D8 Quest Kappa single crystal X-ray diffractometer equipped with an IμS microfocus Mo Kα radiation source (λ = 0.71073 Å) operating at 50 kV and 1 mA. Initial models of the crystal structure were first obtained using SHELXT (intrinsic phasing method) [30] and refined using SHELXL2014 [30]. Final structure refinements include anisotropic displacement parameters and variable occupancy of the Cu site. Additional experimental details are shown in Table 1.

2.4. Magnetism and heat capacity

The temperature dependent DC Magnetic susceptibility $\chi = M/H$ and field dependent magnetization $M(H)$ were measured for a powder sample of $PrCu_{0.45}Te_2$ between T = 2–300 K using a field H = 5000 G and at T = 5 K for H < 7 T. Measurements were performed with a Quantum Design Magnetic Properties Measurement System. The temperature dependent heat capacities, C, for $LaCu_{0.40}Te_2$ and $PrCu_{0.45}Te_2$ were measured using the standard relaxation technique in a Quantum Design Physical Properties Measurement System. Measurements were performed under temperatures ranging between T = 0.4–50 K at zero magnetic field.

3. Results and discussion

3.1. Crystal structure

The ternary chalcogenide $PrCu_{0.45}Te_2$ is isostructural to $LnCu_xTe_2$ (Ln = La, Nd, Sm, Gd, Dy; $x \le 0.4$) [26,31]. The crystal structure of $PrCu_{0.45}Te_2$ from perspectives perpendicular to the *ab*- and *bc*-planes is shown in Fig. 1. The Te2 atoms form quasi one-dimensional chains along the *c*-axis. Te2–Te2 bond distances decrease from 3.1558(5) Å to 3.0273(3) for $LaCu_{0.40}Te_2$ to $DyCu_{0.32}Te_2$, respectively [26]. The Te2–Te2 interatomic distance found in $PrCu_{0.45}Te_2$ is 3.1171(8) Å, which follows the Te2-Te2 distance trend in $LnCu_xTe_2$.

With a cutoff distance of 3.3 Å, the Pr ions are centered in polyhedra comprised of 4 Cu, 4 Te1 and 4 Te2 atoms. The Pr-Cu distances range from 3.162(3) to 3.259(3) Å, which is similar to $PrCu_{13}$, featuring Pr-Cu distances of ~ 3.275 Å [32]. The 4 Pr-Te1 distances are 2 × 3.3175(7), 1 × 3.1620(10) and 1 × 3.1496(13) Å while Pr—Te2

Table 2
Atomic coordinates, site occupancies, and equivalent isotropic displacement parameters for $PrCu_{0.45}Te_2$.

Atom	Wyckoff Site	x	y	z	Occupancy	U_{eq} [a]
Pr	4*d*	0.23882(4)	0.55977(4)	¼	1.0	0.01293(13)
Cu	8*e*	0.4104(4)	0.2043(4)	0.0677(6)	0.222(3)	0.0323(11)
Te1	4*d*	0.61690(5)	0.40882(5)	¼	1.0	0.01049(13)
Te2	4c	0.07939(5)	¼	0	1.0	0.01169(13)

[a] U_{eq} is defined as one third of the trace of the orthogonalized U_{ij} tensor.

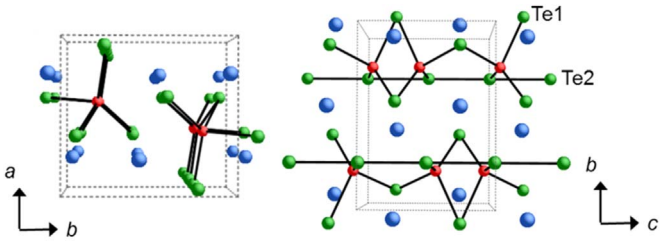

Fig. 1. The structure of $PrCu_{0.45}Te_2$ down the *c*-axis on left and along the *bc*-plane on right. The one-dimensional Te chain runs along the *c*-axis. Blue, red and green spheres represent Pr, Cu, and Te, respectively.

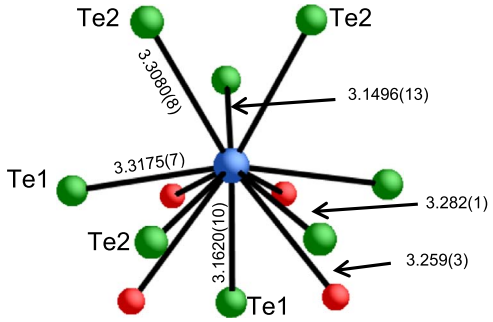

Fig. 2. The coordination environment of Pr is comprised of 4 Cu, 4 Te1, and 4 Te2 atoms. Pr, Cu and Te are represented by blue, red and green spheres, respectively. Numbers represent interatomic distances in Å.

interatomic distances measure 2 × 3.3080(8) and 2 × 3.2819(10) Å. These Pr–Te interatomic distances are similar to Pr–Te bond distances of 3.1537–3.2381 Å found in $PrTe_2$ [33].

$CuTe_4$ tetrahedral units are connected by alternating edge and corner sharing Te1 atoms along the *c*-axis, as depicted in Fig. 3. $CuTe_4$ tetrahedral coordination has been observed in many chalcogenides such as $RCuTe_2$ (*R* = Y, Gd-Lu) [10–12,34–37], $CsCuUTe_3$ [23], $BaAg_8Cu_{2-\delta}Te_2$ [38], Cr_2CuX_4 (X = *S*, Se, Te) [39], $CsCuNd_2Se_4$ [40] and $CsCuGd_2Te_4$ [41]. Cu-Te bond distances in $PrCu_{0.45}Te_2$, shown in Fig. 3, range from 2.595(3) Å to 2.751(3) Å, resulting in distorted $CuTe_4$ tetrahedra. These distances are similar to Cu-Te distances of 2.345–2.682 Å in $Ba_3Cu_{4-x}Te_5$ [42], 2.583–2.593 Å in $KCuZrTe_3$ [43], and 2.671 Å in $Cu_{0.66}EuTe_2$ [44]. In $PrCu_{0.45}Te_2$ the shortest Cu-Cu interatomic distances between partially occupied, symmetry equivalent sites are only 1.145(8) and 2.273(8) Å. To the best of our knowledge,

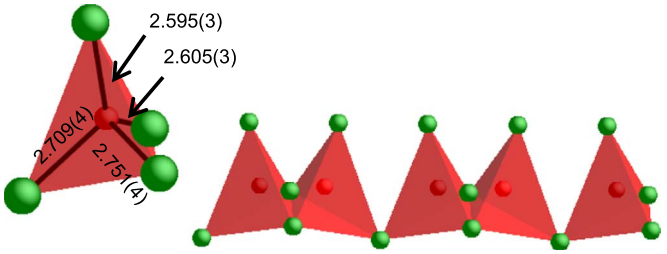

Fig. 3. Left: A distorted $CuTe_4$ tetrahedron with bond distances shown in Å. Right: Edge and corner sharing $CuTe_4$ chain along the *c*-axis.

the shortest known Cu-Cu separation is 2.35 Å (in Cu(tolyl-NNNNN-tolyl)$_3$) [45]; hence, it is plausible that the Cu atoms are geometrically constrained and that $CuTe_4$ tetrahedra share only corners in the local crystal structure.

One significant observation to note is that the U_{eq} of Cu was three times larger than U_{eq} values of Pr and Te in single crystal X-ray diffraction experiments. The U_{eq} of Cu is highly anisotropic with U_{33} being approximately twice that of U_{11} and U_{22}. The ~ 3.21 and ~3.96 Å Cu···Cu distances in $PrCu_{0.45}Te_2$ are somewhat larger than Cu···Cu distances of ~ 2.8–3.1 Å observed in NaCuTe [46] and $NaCu_3Te_2$ [47], which contain ordered $CuTe_4$ tetrahedral chains and layers. The unusual atomic displacement parameter (ADP) of Cu may be due to the random variation of the Cu···Cu distances in the average structure. Further investigation of the local structure would provide insight into the nature of Cu bonding. It should be noted that the Cu ADP is large relative to other atoms only in $PrCu_{0.45}Te_2$. In other previously published rare-earth analogues of this structure type, the Cu ADP are similar to atomic displacement parameters of the rare-earth and Te atoms, except for the Gd and Dy analogues where the Cu ADP is approximately double the ADPs of the other atoms [26].

3.2. Magnetic susceptibility

The temperature dependent DC magnetic susceptibility $\chi = M/H$ and field dependent magnetization M(*H*) were measured for a powder sample of $PrCu_{0.45}Te_2$ between T = 2–300 K using a field *H* = 5000 G and at *T* = 5 K for *H* < 7 T (Fig. 4). Across nearly the entire temperature range, the magnetic susceptibility data follow a Curie-Weiss temperature dependence, $\chi = (C/(T-\theta))$, where *C* is the Curie constant and θ is the Curie-Weiss temperature (Fig. 4b). The weak deviation from this function only at low temperatures reveals that the impact of crystal electric field splitting on the magnetic state is weak. A fit to the data on the range *T* = 50–300 K yields the values *C* = 1.44 cm^3K/mol and θ = -11.4 K. From *C*, the effective magnetic moment μ_{eff} is calculated to be 3.4 μ_B, which is close to the theoretical value of 3.51 μ_B for Pr^{3+}. From this, it was concluded that the magnetism of this system is

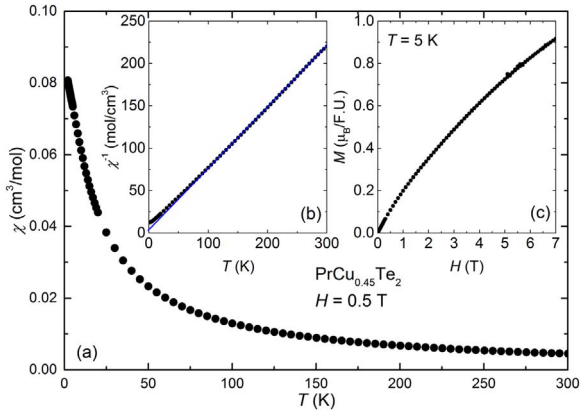

Fig. 4. (a) The temperature dependent magnetic susceptibility $\chi = M/H$ vs temperature *T* collected in an applied magnetic field *H* = 0.5 T for $PrCu_{0.45}Te_2$. (b) Inverse magnetic susceptibility χ^{-1}(T). The straight blue line is a Curie-Weiss fit to the data, as described in the text. (c) Field dependent magnetization of $PrCu_{0.45}Te_2$ at 5 K.

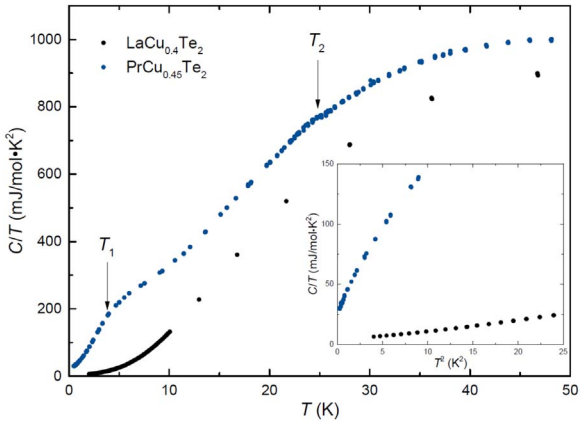

Fig. 5. Comparison between the heat capacity divided by temperature C/T vs T for $LaCu_{0.40}Te_2$ and $PrCu_{0.45}Te_2$. Inset: C/T vs T^2 for both compounds.

associated with the 4f-electrons of Pr and that the Cu 3d-electrons do not carry a localized moment. Although there is no evidence for magnetic ordering, the modest and negative θ has been found to provide evidence for antiferromagnetic exchange between the *f*-electron moments. The field dependence of the magnetization at $T = 5$ K (Fig. 4c) is consistent with this scenario, where a gradual increase with negative curvature is observed, to approach a moment near 0.9 μ_B/formula unit (F.U.) at $H = 7$ T.

3.3. Heat capacity

The temperature dependence of the heat capacity divided by temperature C/T vs T for $PrCu_{0.45}Te_2$ and its nonmagnetic analogue $LaCu_{0.40}Te_2$ are shown in Fig. 5. $LaCu_{0.40}Te_2$ exhibits a typical temperature dependence, where the low T behavior follows the expression $C/T = \gamma + \beta T^2$ (γ and β are the electronic and phonon contributions to the heat capacity, respectively) with $\gamma_{La} = 3.1$ mJ/mol K^2 and $\beta = 0.78$ mJ/mol K^2 (Fig. 5 inset). From the non-zero value of γ_{La}, it has been concluded that there are an appreciable number of charge carriers near the Fermi energy. This is unexpected since earlier work shows that the chemical analogues exhibit semiconducting behavior, where γ would be close to zero. From the value of β, the Debye temperature has been calculated $\theta_D = 215$ K. In contrast, $PrCu_{0.45}Te_2$ exhibits a strong enhancement of C/T across the entire measured temperature range with nonmonotonic features. In particular, there is a clear but broad hump around $T_1 \approx 4$ K and a much weaker hump around $T_2 \approx 24$ K. These anomalies could indicate short range magnetic ordering. A linear extrapolation of the low temperature behavior also suggests that $\gamma_{Pr} \approx 27$ mJ/mol·K^2, which is much larger than γ_{La}. It is natural to associate this difference with the unquenched entropy of the Pr *f*-moments, and similar anomalous behavior is frequently associated with the development of either spin glass states or correlated spin liquids [48]. In fact $C \propto T^2$ was reported for $Lu_2Mo_2O_7$ which is observed to display an anomalous spin glass state in the absence of any significant chemical or bond disorder [49]. Thermal transport measurements may help in understanding the nature of the heat capacity observed for $PrCu_{0.45}Te_2$.

4. Discussion and conclusions

Taken together, these results expose $PrCu_{0.45}Te_2$ as a disordered magnetic semiconductor. Since the La analogue is also a semiconductor, it is clear that the electronic behavior is a result of the band structure which does not seem to be influenced by the flat f-states which, in principle, could be near the Fermi energy. Instead, the Pr ions carry a localized trivalent moment indicating that they are well below the Fermi energy. From the viewpoint of the magnetic susceptibility, this produces a typical Curie-Weiss behavior with a small antiferromagnetic exchange interaction on the order of θ = -11.4 K. This would lead us to expect magnetic ordering around this temperature, but instead we find no evidence for a phase transition. In its place, there is an unexpected build-up of the heat capacity that is centered around $T_1 \approx 4$ K. This may represent short range magnetic ordering resulting from magnetic frustration, but further work is needed to clarify the origin of this behavior. It should be pointed out that theoretical calculations show that the Cu-Te interactions in $LaCu_xTe_2$ ($0.28 \le x \le 0.50$) play an important role in its electronic band structure; distortions in the Te chain resulting from varying Cu concentrations resulted in a band gap opening at the Fermi energy [50]. In light of these calculations, the larger atomic displacement parameters of Cu site in our diffraction studies of $PrCu_{0.45}Te_2$ warrants further investigation into the local structure of Cu and its effects on magnetic frustration of the Pr network. It should be noted that preliminary transport measurements reveal very high resistivities suggesting that this system is also semiconducting.

Acknowledgements

RTM acknowledges National Science Foundation CAREER Award 1541230 and JYC acknowledges National Science Foundation Division of Materials Research 1700030 for partial support of this project. LB is supported by Department of Energy Basic Energy Science through award Department of Energy SC0002613. A portion of this work was performed at the National High Magnetic Field Laboratory (NHMFL), which is supported by National Science Foundation Cooperative Agreements No. Division of Materials Research 1157490 and No. Division of Materials Research 1644779 and the state of Florida. RTM thanks Sau Doan Nguyen for useful discussions.

Appendix A. Supplementary material

Supplementary data associated with this article can be found in the online version at doi:10.1016/j.jssc.2018.10.008.

References

[1] T. Chivers, Tellurium compounds of the main-group elements: progress and prospects, Dalton Trans. (1996) 1185–1194.
[2] R. Patschke, M.G. Kanatzidis, Polytelluride compounds containing distorted nets of tellurium, Phys. Chem. Chem. Phys. 4 (2002) 3266–3281.
[3] S. Seong, T.A. Albright, X. Zhang, M. Kanatzidis, Te-Te bonding in copper tellurides, J. Am. Chem. Soc. 116 (1994) 7287–7293.
[4] K. Mitchell, J.A. Ibers, Rare-earth transition-metal chalcogenides, Chem. Rev. 102 (2002) 1929–1952.
[5] O. Mayasree, C.R. Sankar, K.M. Kleinke, H. Kleinke, Cu clusters and chalcogen-chalcogen bonds in various copper polychalcogenides, Coord. Chem. Rev. 256 (2012) 1377–1383.
[6] C. Malliakas, S.J.L. Billinge, H.J. Kim, M.G. Kanatzidis, Square nets of tellurium: rare-earth dependent variation in the charge-density wave of $RETe_3$ (RE = rare-earth element), J. Am. Chem. Soc. 127 (2005) 6510–6511.
[7] C.D. Malliakas, M.G. Kanatzidis, Charge density waves in the square nets of tellurium of $AMRETe_4$ (A = K, Na; M = Cu, Ag; RE = La, Ce), J. Am. Chem. Soc. 129 (2007) 10675–10677.
[8] G.J. Snyder, E.S. Toberer, Complex thermoelectric materials, Nat. Mater. 7 (2008) 105–114.
[9] R. Patschke, J. Heising, P. Brazis, C.R. Kannewurf, M. Kanatzidis, $KCuCeTe_4$: a new intergrowth rare earth telluride with an incommensurate superstructure associated with a distorted square net of tellurium, Chem. Mater. 10 (1998) 695–697.
[10] M. Esmaeili, S. Forbes, Y.-C. Tseng, Y. Mozharivskyj, Crystal structure, electronic and physical properties of monoclinic $RECuTe_2$ in contrast to $RECuSe_2$ (RE = Pr, Sm, Gd, Dy and Er), Solid State Sci. 186 (2014) 142–148.
[11] H. Lin, H. Chen, J.-N. Shen, L. Chen, L.-M. Wu, Chemical modification and energetically favorable atomic disorder of a layered thermoelectric material $TmCuTe_2$ leading to high performance, Chem. Eur. J. 20 (2014) 15401–15408.
[12] H. Lin, H. Chen, N. Ma, Y.J. Zheng, J.N. Shen, J.S. Yu, X.T. Wu, L.M. Wu, Syntheses, structures, and thermoelectric properties of ternary tellurides: $RECuTe_2$ (RE = Tb-Er), Inorg. Chem. Front. 4 (2017) 1273–1280.
[13] M.N. Ali, J. Xiong, S. Flynn, J. Tao, Q.D. Gibson, L.M. Schoop, T. Liang, N. Haldolaarachchige, M. Hirschberger, N.P. Ong, R.J. Cava, Large, non-saturating magnetoresistance in WTe_2, Nature 514 (2014) 205–208.
[14] D. Kang, Y. Zhou, W. Yi, C. Yang, J. Guo, Y. Shi, S. Zhang, Z. Wang, C. Zhang,

S. Jiang, A. Li, K. Yang, Q. Wu, G. Zhang, L. Sun, Z. Zhao, Superconductivity emerging from a suppressed large magnetoresistant state in tungsten ditelluride, Nat. Commun. 6 (2015) 7804.
[15] I. Belopolski, D.S. Sanchez, Y. Ishida, X.C. Pan, P. Yu, S.Y. Xu, G.Q. Chang, T.R. Chang, H. Zheng, N. Alidoust, G. Bian, M. Neupane, S.M. Huang, C.C. Lee, Y. Song, H.J. Bu, G.H. Wang, S.S. Li, G. Eda, H.T. Jeng, T. Kondo, H. Lin, Z. Liu, F.Q. Song, S. Shin, M.Z. Hasan, Discovery of a new type of topological Weyl fermion semimetal state in $Mo_xW_{1-x}Te_2$, Nat. Commun. 7 (2016) 13643.
[16] A. Tamai, Q.S. Wu, I. Cucchi, F.Y. Bruno, S. Ricco, T.K. Kim, M. Hoesch, C. Barreteau, E. Giannini, C. Besnard, A.A. Soluyanov, F. Baumberger, Fermi arcs and their topological character in the candidate type-II Weyl semimetal $MoTe_2$, Phys. Rev. X 6 (2016) 031021.
[17] A.A. Soluyanov, D. Gresch, Z.J. Wang, Q.S. Wu, M. Troyer, X. Dai, B.A. Bernevig, Type-II Weyl semimetals, Nature 527 (2015) 495–498.
[18] Z.J. Wang, D. Gresch, A.A. Soluyanov, W.W. Xie, S. Kushwaha, X. Dai, M. Troyer, R.J. Cava, B.A. Bernevig, MoTe2: a type-II Weyl topological metal, Phys. Rev. Lett. 117 (2016) 056805.
[19] Y. Sun, S.C. Wu, M.N. Ali, C. Felser, B.H. Yan, Prediction of Weyl semimetal in orthorhombic $MoTe_2$, Phys. Rev. B 92 (2015) 161107.
[20] J. Janek, Mixed conductors: the bridge to redox switches, Nat. Mater. 8 (2009) 88–89.
[21] W.-H. Jiao, Z.-T. Tang, Y.-L. Sun, Y. Liu, Q. Tao, C.-M. Feng, Y.-W. Zeng, Z.-A. Xu, G.-H. Cao, Superconductivity in a layered $Ta_4Pd_3Te_{16}$ with $PdTe_2$ Chains, J. Am. Chem. Soc. 136 (2014) 1284–1287.
[22] O. Mayasree, Y. Cui, A. Assoud, H. Kleinke, Structure change via partial Se/Te substitution: crystal structure and physical properties of the telluride $Ba_2Cu_{4-x}Te_5$ in contrast to the selenide-telluride $Ba_2Cu_{4-x}Se_yTe_{5-y}$, Inorg. Chem. 49 (2010) 6518–6524.
[23] J.A. Cody, J.A. Ibers, Uranium tellurides: new one- and two-dimensional compounds $CsUTe_6$, $CsTiUTe_5$, $Cs_8Hf_5UTe_{30.6}$, and $CsCuUTe_3$, Inorg. Chem. 34 (1995) 3165–3172.
[24] J.A. Cody, J.A. Ibers, Synthesis and structure of the layered thorium telluride $CsTh_2Te_6$, Inorg. Chem. 35 (1996) 3836–3838.
[25] F.Q. Huang, J.A. Ibers, $Gd_3Cu_2Te_7$ and $U_2Cu_{0.78}Te_6$: two examples of linear Te chains, J. Solid State Chem. 159 (2001) 186–190.
[26] F.Q. Huang, P. Brazis, C.R. Kannewurf, J.A. Ibers, Syntheses, structures, physical properties, and theoretical study of $LaCu_{0.40}Te_2$, $NdCu_{0.37}Te_2$, $SmCu_{0.34}Te_2$, $GdCu_{0.33}Te_2$, and $DyCu_{0.32}Te_2$, J. Am. Chem. Soc. 122 (2000) 80–86.
[27] J. von Boehm, P. Bak, Devil's stairs and the commensurate-commensurate transitions in CeSb, *Phys. Rev. Lett.* 42 (979) 122-125.
[28] K.W. Chen, Y. Lai, Y.C. Chiu, S. Steven, T. Besara, D. Graf, T. Siegrist, T.E. Albrecht-Schmitt, L. Balicas, R.E. Baumbach, Possible devil's staircase in the Kondo lattice CeSbSe, Phys. Rev. B 96 (2017) 014421.
[29] L.M. Schoop, A. Topp, J. Lippmann, F. Orlandi, L. Müchler, M.G. Vergniory, Y. Sun, A.W. Rost, V. Duppel, M. Krivenkov, S. Sheoran, P. Manuel, A. Varykhalov, B. Yan, R.K. Kremer, C.R. Ast, B.V. Lotsch, Tunable Weyl and Dirac states in the nonsymmorphic compound CeSbTe, Sci. Adv. 4 (2018).
[30] G. Sheldrick, Crystal structure refinement with SHELXL, Acta Crystallogr., Sect. C. 71 (2015) 3–8.
[31] N.-H. Dung, M.-P. Pardo, P. Boy, Single-crystal structure of copper lanthanum telluride $Cu_{0.28}LaTe_2$: a disordered tunnel structure, Acta Cryst. Sect. C. 39 (1983) 668–670.
[32] J.M. Bloch, D. Shaltiel, D. Davidov, Preparation and study of new intermetallic compounds with the $NaZn_{13}$ structure: LaCu13, PrCu13, J. Less Common Met. 79 (1981) 323–327.
[33] G.V. Lashkarev, Y.B. Paderno, Physical properties and chemical bond in rare-earth chalcogenides, Izv. Akad. Nauk SSSR, Neorg. Mater. 1 (1965) 1791–1802.
[34] V.Y. Shemet, L.D. Gulay, J. Stepien-Damm, A. Pietraszko, I.D. Olekseyuk, Investigation of the Y_2Te_3–Cu_2Te–PbTe system at 870K and crystal structures of the $Y_7Cu_3Te_{12}$ and $YCu_{0.264}Te_2$ compounds, J. Alloy. Compd. 420 (2006) 58–62.
[35] U. Aydemir, J.-H. Pohls, H. Zhu, G. Hautier, S. Bajaj, Z.M. Gibbs, W. Chen, G. Li, S. Ohno, D. Broberg, S.D. Kang, M. Asta, G. Ceder, M.A. White, K. Persson, A. Jain, G.J. Snyder, $YCuTe_2$: a member of a new class of thermoelectric materials with $CuTe_4$-based layered structure, J. Mater. Chem. 4 (2016) 2461.
[36] E.M. Godzhaev, O.M. Aliev, V.A. Mamedov, M.M. Zarbaliev, Synthesis and study of copper lanthanide telluride ($CuLnTe_2$) compounds, Izv. Akad. Nauk. SSSR, Neorg. Mater. 13 (1977) 441–443.
[37] L.D. Gulay, M. Daszkiewicz, V.Y. Shemet, Crystal structure of ~RCu_3S_3 and ~$RCuTe_2$ (R=Gd–Lu) compounds, J. Solid State Chem. 186 (2012) 142–148.
[38] A. Assoud, Y. Cui, S. Thomas, B. Sutherland, H. Kleinke, Structure and physical properties of the new telluride $BaAg_2Te_2$ and its quaternary variants $BaCu_8Ag_{2-8}Te_2$, J. Solid State Chem. 181 (2008) 2024–2030.
[39] J.B. Goodenough, Tetrahedral-site copper in chalcogenide spinels, Solid State Commun. 5 (1967) 577–580.
[40] J.-M. Babo, S. Strobel, T. Schleid, Z. Anorg. Allg. Chem. 636 (2010) 349–355.
[41] M. Zelinska, A. Assoud, H. Kleinke, Synthesis, crystal and electronic structure, and physical properties of the new lanthanum copper telluride $La_3Cu_5Te_7$, J. Solid State Chem. 184 (2011) 516–522.
[42] A. Assoud, S. Thomas, B. Sutherland, H.Q. Zhang, T.M. Tritt, H. Kleinke, Thermoelectric properties of the new polytelluride $Ba_3Cu_{14}.dTe_{12}$, Chem. Mater. 18 (2006) 3866–3872.
[43] M.F. Mansuetto, P.M. Keane, J.A. Ibers, Synthesis, structure, and conductivity of the new group-IV chalcogenides, $KCuZrQ_3$ (Q = *S*, Se, Te), J. Solid State Chem. 101 (1992) 257–264.
[44] R. Patschke, P. Brazis, C.R. Kannewurf, M.G. Kanatzidis, $Cu_{0.66}EuTe_2$, KCu_2EuTe_4 and $Na_{0.2}Ag_{2.8}EuTe_4$: compounds with modulated square Te nets, J. Mater. Chem. 9 (1999) 2293–2296.
[45] J. Beck, J. Strahle, Complexes of 1,5-di(p-tolyl)–1,4-pentaazadien-3ide, crystal structures of $[Cu(tolyl\text{-}NNNNN\text{-}tolyl)]_3$ and $Ni[(tolyl(NNNNN\text{-}tolyl)_2]_2$ Angew, Chem., Int. Ed. Engl. 24 (1985) 409–410.
[46] G. Savelsberg, Ternäre pnictide und chalkogenide von alkalimetallen und IB-bzw. IIB-elementen / On ternary pnictides and chalkogenides of alkaline metals and IB-resp. II B-elements, Z. Naturforsch. B 33 (1978) 370.
[47] K.O. Klepp, Preparation and crystal structure of $NaCu_3Te_2$, Z. Naturforsch. B 42 (1987) 130–134.
[48] Y. Li, H. Liao, Z. Zhang, S. Li, F. Jin, L. Ling, L. Zhang, Y. Zou, L. Pi, Z. Yang, J. Wang, Z. Wu, Q. Zhang, Gapless quantum spin liquid ground state in the two-dimensional spin−1/2 triangular antiferromagnet $YbMgGaO_4$, Sci. Rep. 5 (2015) 16419.
[49] L. Clark, G.J. Nilsen, E. Kermarrec, G. Ehlers, K.S. Knight, A. Harrison, J.P. Attfield, B.D. Gaulin, From spin glass to quantum spin liquid ground states in molybdate pyrochlores, Phys. Rev. Lett. 113 (2014) 117201.
[50] F.C. Gladisch, S. Steinberg, Revealing the nature of bonding in rare-arth transition-metal tellurides by means of methods based on first principles, Eur. J. Inorg. Chem. 2017 (2017) 3395–3400.